

Towards asteroseismically calibrated age-rotation-activity relations for *Kepler* solar-like stars

R. A. García¹, T. Ceillier¹, D. Salabert¹, S. Mathur², J. L. van Saders³, M. Pinsonneault³, J. Ballot^{4,5}, P. G. Beck^{1,6}, S. Bloemen⁷, T. L. Campante⁸, G. R. Davies^{1,8}, J.-D. do Nascimento Jr.^{9,10}, S. Mathis¹, T. S. Metcalfe^{2,11}, M. B. Nielsen^{12,13}, J. C. Suárez¹⁴, W. J. Chaplin⁸, A. Jiménez^{15,16}, and C. Karoff¹¹

- ¹ Laboratoire AIM, CEA/DSM – CNRS – Univ. Paris Diderot – IRFU/SAP, Centre de Saclay, 91191 Gif-sur-Yvette Cedex, France
² Space Science Institute, 4750 Walnut Street, Suite 205, Boulder, CO 80301, USA
³ Department of Astronomy, The Ohio State University, Columbus, Ohio 43210, USA
⁴ CNRS, Institut de Recherche en Astrophysique et Planétologie, 14 avenue Edouard Belin, 31400 Toulouse, France
⁵ Université de Toulouse, UPS-OMP, IRAP, 31400 Toulouse, France
⁶ Instituut voor Sterrenkunde, Katholieke Universiteit Leuven, Celestijnenlaan 200D, B-3001 Leuven, Belgium
⁷ Department of Astrophysics, IMAPP, Radboud University Nijmegen, PO Box 9010, NL-6500 GL Nijmegen, The Netherlands
⁸ School of Physics and Astronomy, University of Birmingham, Edgbaston, Birmingham B15 2TT, UK
⁹ Harvard-Smithsonian Center for Astrophysics, Cambridge, Massachusetts 02138, USA
¹⁰ U. Federal do Rio Grande do Norte, UFRN, Dep. de Física Teórica e Experimental, DFTE, CP 1641, 59072-970, Natal, RN, Brazil
¹¹ Stellar Astrophysics Centre, Dept. of Physics and Astronomy, Aarhus Univ., Ny Munkegade 120, DK-8000 Aarhus C, Denmark
¹² Institut für Astrophysik, Georg-August-Universität Göttingen, Friedrich-Hund-Platz 1, 37077, Göttingen, Germany
¹³ Max Planck Institute for Solar System Research Justus-von-Liebig-Weg 3 37077 Göttingen, Germany
¹⁴ Instituto de Astrofísica de Andalucía (CSIC), 3004, Granada, Spain
¹⁵ Universidad de La Laguna, Dpto de Astrofísica, 38206, Tenerife, Spain
¹⁶ Instituto de Astrofísica de Canarias, 38205, La Laguna, Tenerife, Spain

Received 01 January 1901/ Accepted 01 January 1901

ABSTRACT

Context. *Kepler* ultra-high precision photometry of long and continuous observations provide a unique dataset in which surface rotation and variability can be studied for thousands of stars. Because many of these old field stars also have independently measured asteroseismic ages, measurements of rotation and activity are particularly interesting in the context of age-rotation-activity relations. Age-rotation relations generally lack good calibrators at old ages, a problem that this *Kepler* sample of old field stars is uniquely suited to address.

Aims. We study the surface rotation and the photometric magnetic activity of a subset of 540 solar-like stars on the main-sequence and the subgiant branch for which stellar pulsations have been measured, and establish new calibrations for age-rotation and age-activity relations.

Methods. The rotation period is determined by comparing the results from two different analysis methods: i) The projection into the frequency domain of the time-period analysis using a Morlet wavelet, in which the rotation period is estimated by studying the highest peaks in the Global Wavelet Power Spectrum (GWPS) through the least-squared fit of a combination of gaussian functions, ii) The autocorrelation function (ACF) of the light curves. Reliable surface rotation rates can then be extracted by comparing the results from two different sets of calibrated data and from the two complementary aforementioned analyses. Global photometric levels of magnetic activity in this sample of stars are also extracted by using a photometric activity index, which takes into account the rotation period of the stars.

Results. Out of the 540 solar-like pulsating stars in our sample, we successfully measured the rotation period of 310 stars (excluding known binaries and candidate planet host stars). The rotation periods lay between 1 and 100 days. The remaining stars are classified into two categories: those not showing any surface rotation (6 stars), and those in which the four analyses did not converge to a single and robust rotation period (213). The photometric magnetic activity levels of these 310 solar-like pulsating stars were computed and for 61.5% of the dwarfs, its value is comparable to the solar one. We then extract age-rotation only for the dwarfs in our sample with very precise asteroseismic age estimations, highlighting the necessity of excluding the hot stars and the subgiants when inferring such relations. We also studied age-activity-rotation relations with a hint of correlation for the subgiants.

Key words. Asteroseismology - Stars: rotation - Stars: activity - Stars: solar-type - Stars: evolution - Stars: oscillations - Kepler

1. Introduction

Stellar rotation fundamentally modifies stellar interiors (e.g. Zahn 1992; Pinsonneault 1997; Mathis & Zahn 2004; Decressin et al. 2009; Eggenberger et al. 2010; Ceillier et al. 2013; Marques et al. 2013). When it is considered in the stellar evolution models, the inferred age of the star is modified, which has severe consequences, for example, in planetary systems (e.g.

Pinsonneault 2009). Surface rotation can also be used as an observable to determine the age of the star. Gyrochronology –the empirical relationship between rotation period, color, and age (e.g. Barnes 2007; Charnamé & Ramírez 2012) – provides means by which surface rotation can be used to infer ages of cool stars (e.g. Barnes 2009; Meibom et al. 2011a). These relationships,

however, must be calibrated, and rely on systems in which both rotation periods and stellar ages can be independently measured.

During the last decades, the detailed knowledge of stellar evolution has been improved thanks to the observational constraints provided by helio- and asteroseismology (e.g. Christensen-Dalsgaard 2010). Solar-type stars are those that show global physical characteristics similar to the Sun. In particular, they have stochastically excited modes due to the presence of an outer convective envelope (e.g. Goldreich & Keeley 1977; Goldreich et al. 1994; Belkacem et al. 2008).

Solar-type stars are generally slow rotators (in most cases $v \sin i < 20 \text{ km s}^{-1}$) and the influence of rotation on the oscillation frequencies is well known. However, distortion due to the centrifugal force can have a large impact on the oscillation frequencies even for slow rotators (e.g. Goupil 2009; Reese 2010, and references therein). Such an effect is stronger for acoustic (p) modes with small inertia, which have a higher sensitivity to the outer layers of the star. Therefore, their frequencies are more sensitive to the physical properties of the surface, where the centrifugal force becomes more efficient (e.g. Suárez et al. 2010; Ouazzani & Goupil 2012). The induced perturbations are of the same order of magnitude –or even larger– as the effects of turbulence or diffusion, currently considered the origin of the so-called surface effects. It is thus important to study the surface rotation of other stars that are similar to the Sun and have larger rotational velocities. This could allow us to better understand the role of rotation in comparison to other surface effects and, hence, to properly interpret the oscillation spectra of solar-like stars, at least in the high-frequency domain.

With the advent of the detection of mixed modes in subgiant and giant stars (e.g. Beck et al. 2011; Bedding et al. 2011; Mosser et al. 2011; Stello et al. 2013; Benomar et al. 2013, 2014) –including some belonging to a few clusters (Stello et al. 2011; Basu et al. 2011)– it is now possible to infer the rotation rate of the core of these stars (Beck et al. 2012; Mosser et al. 2012; Di Mauro et al. 2013; Goupil et al. 2013), which is still difficult for solar-like stars and even for the Sun (e.g. García et al. 2004, 2007, 2008a). In a few cases it is not only possible to obtain an averaged internal rotation rate (e.g. Gizon et al. 2013; Mathur et al. 2013; Chaplin et al. 2013), but indications of the rotation profile from the external outer convection zone to the inner radiative core using inversion techniques (Deheuvels et al. 2012, 2014; Beck et al. 2013), as it is also commonly done for the Sun (e.g. Thompson et al. 2003; García et al. 2008b; Mathur et al. 2008; Eff-Darwich & Korzennik 2013). Unfortunately, in the stellar case –as only low-degree modes are observable– the inversion is increasingly uncertain close to the surface and measurements of the surface rotation rate are required. A better knowledge of the rotation profiles would be fundamental to answering long-standing questions about stellar interiors, transport of angular momentum, and rotational mixing. Hence the seismic analysis and the complementary study of the surface rotation are crucial.

High-quality photometric time series obtained by the *Kepler* mission (Borucki et al. 2010; Koch et al. 2010) can be used to study the surface rotation and magnetic activity of solar-like stars in which eigenmodes are measured. Indeed, when a star is active (e.g. García et al. 2010; Lanza 2010), starspots periodically cross the visible stellar disk. This produces a modulation in the brightness of the star that can be measured (e.g. Mosser et al. 2009a; García et al. 2012; do Nascimento et al. 2012). The time evolution of such fluctuations provides a measurement of the surface velocity at the latitudes of the spots (e.g. García et al. 2009; Ballot et al. 2011; McQuillan et al. 2013a; Nielsen et al.

2013), which can also lead to the determination of the surface differential rotation (e.g. Barban et al. 2009; Mosser et al. 2009b; Mathur et al. 2010a; Fröhlich et al. 2012; Reinhold & Reiners 2013; Lanza et al. 2014).

The photometric variability of stars observed by *Kepler* (e.g. Basri et al. 2010, 2013) can be related to the surface magnetism at the time scales associated with the rotation periods. Therefore, the amplitude of the photometric modulation in the light curve can be used as an indicator of the surface magnetic variability as recently demonstrated for the Sun (e.g. García et al. 2013b; Mathur et al. 2014b), on long and short timescales. Using a variability metric directly obtained from the light curve, Campante et al. (2014) confirmed that amplitudes of solar-like oscillations are suppressed in stars with increased levels of surface magnetic activity.

In the present work, we study the surface rotation rate and the photometric magnetic variability in the subset of 540 *Kepler* solar-like stars studied by Chaplin et al. (2014), for which accurate fundamental global parameters such as radius, masses, and ages have been inferred from the combination of asteroseismic and photometric observations. This seismic stellar sample has the potential impact on the field of gyrochronology, in which stellar rotation periods are used as a proxy for age. The period-age relations are empirically calibrated with stellar systems for which independent ages and rotation periods are measured. Several calibrations already exist in the literature (Pace & Pasquini 2004; Barnes 2007; Mamajek & Hillenbrand 2008; Meibom et al. 2009, 2011b), but consistently struggle to find a calibration set at old ages and long rotation periods. *Kepler* light curves provide means to measure both the stellar age through asteroseismology, and the rotation periods through spot modulation for an old field star population, and as such represents an important contribution to the gyrochronological calibrators.

We describe the preparation of the *Kepler* light curves in Section 2, analyse the extracted rotation periods in Section 3 and study the projected magnetic activity levels in Section 4. The discussion of the results follows in Section 5.

2. Observations and data analysis

In the present study, we use data collected by the NASA planet-hunter *Kepler* mission. The satellite is placed in a 372.5-d Earth-trailing heliocentric orbit. To keep the solar panels and the radiators which cool down the focal plane correctly aligned with respect to the Sun, *Kepler* performs 90° rolls along its axis every 3 months (Haas et al. 2010), producing discontinuities in the observations. The light curves are therefore divided into “*Kepler* quarters”, denoted by Q_n, starting by Q₀ –the initial 10-d-long commissioning run– followed by a 34-d-long first quarter (Q₁), and subsequent 3-month-long quarters (Q₂, Q₃,...). In this work, we use data up to Q₁₄ whenever available for the stars in the sample.

Around 120,000 stars –located in the constellation of Cygnus and Lyra– have been quasi-continuously monitored by *Kepler* during the full mission with a cadence of 29.4244 min (usually called Long Cadence, LC, data). Among all these stars, 512 can be observed with a much faster cadence of 58.84876 s (Short Cadence, SC, data) at any given time. This was done primarily to obtain a more precise timing of planetary transits (Gilliland et al. 2010). However, a subset of around 120 stars among these 512 was reserved for asteroseismic studies by the *Kepler* Asteroseismic Science Consortium (KASC, <http://kasoc.phys.au.dk/>) in order to study main-sequence and subgiant solar-like pulsating stars. During these evolutionary

stages, the p-mode oscillations are located above the Nyquist frequency associated with the sampling rate of the LC data ($283.45 \mu\text{Hz}$). Therefore, the p-mode oscillations in these stars can only be studied using SC data (with a Nyquist frequency of 8.496 mHz) (e.g. Campante et al. 2011; Mathur et al. 2011; Appourchaux et al. 2012; Metcalfe et al. 2012).

For this work, we are interested in extracting the stellar surface rotation for periods longer than 1 day. Thus, we need to have light curves corrected for any low-frequency instrumental perturbations and with all the quarters properly concatenated together. Therefore, we use Simple Aperture Photometry (SAP) time series (Thompson et al. 2013) and we correct outliers, jumps, and drifts following the procedures described in García et al. (2011), usually denoted as KADACS (*Kepler* Asteroseismic Data Analysis and Calibration Software) light curves. These data are high-pass filtered using two triangular smoothing functions with cut-off periods at 30 and 100 days. The latter produces noisier light curves than the 30-days one. Therefore we use the smaller filter when the results are the same and we flag in Table 2 the results obtained with the 100-day-filter light curves. Moreover, to minimize the dependency of the correction software, we also use *Kepler* light curves processed using “Pre Data Conditioning Maximum a Posteriori” methods (PDC-MAP, e.g. Thompson et al. 2013). Unfortunately, this methodology works in a quarter-by-quarter basis, which filters all periods close to 90 days, as well as, sometimes, everything longer than 20 days with a growing attenuation for periods longer than 3 days. Finally, it is important to mention that we avoid the use of the latest *Kepler* data products: “Pre Data Conditioning multi-scale Maximum a Posteriori corrected series” (PDC-msMAP, see for further details Thompson et al. 2013), because each quarter is high-pass filtered with a limit of around 21 days. An example of the application of the three different correction methodologies applied to the same star can be seen in Fig. 1 of García et al. (2013a).

As these corrections are not perfect, some problems can remain in the corrected light curves. To minimise these effects, we remove from the light curves the quarters that show anomalously high variance compared to neighbours. To do so, we compute the variance of every quarter in every light curve and we divide the resulting array by its median. Then, we compute the difference in this ratio between each quarter its two neighbours. If the mean of these two differences is greater than a threshold – empirically set to 0.9 – we remove the quarter from the light curve. This method is applied both to the PDC-MAP and the KADACS light curves to produce the datasets used in this study.

Photometric pollution from nearby stars in the field of view can bias the rotation period estimation. The value of the crowding factor for each target (i.e. the ratio of the target-to-total flux in the optimal aperture) can be used to identify any target with a potential source of bias. Moreover, the crowding factor changes every quarter as *Kepler* rolls along its axis. The median value of the crowding factor over all the observed quarters C_f is then determined. The maximal variation of the crowding factor between each quarter, σ_{C_f} , is used as an indication of the associated uncertainty. The left panel of Fig. 1 shows the crowding C_f values for all the 540 targets in the analysed sample as a function of the *Kepler* magnitude Kp , while the right panel of Fig. 1 shows the associated uncertainties, σ_{C_f} . The majority of the stars have a value of C_f between 1 and 0.98, and, therefore, we can postulate that they are not affected by pollution of another star in the field. Six of them appear as outliers with C_f around 0.95. The pixel data of these stars were checked, validating their photometry. Only one star ($Kp=11.0$) is out of the represented y range: KIC 7938112, with a $C_f = 0.73 \pm 0.16$. The analysis of

its power spectrum shows two humps of p-mode power, one corresponding to a solar-like star at high frequency and another at low frequency corresponding to a red giant. Hence, this could be an example of a possible seismic binary or a case of a contaminated flux by a nearby red giant.

3. Analysing the surface rotation

Several methods can be used to look for the average rotation rate of the stellar surface due to the motion of starspots across the visible stellar disk. This periodicity can be measured by extracting the highest peak in the low-frequency part of the periodogram as done by Nielsen et al. (2013). They studied thousands of dwarfs (from F to M-type stars) observed by the *Kepler* mission during eight consecutive quarters, but analyzed each one independently, which limited their analysis to periods in the range from 1 to 30 days. Reinhold et al. (2013) also studied the low-frequency part of the periodogram –computed using only Q3 data– to extract rotation periods and differential rotation for almost 20,000 targets in a wider range of periods from 0.5 to 45 days. Unfortunately, the highest peak in the periodogram can sometimes be a higher overtone of the fundamental rotation period and the extracted rotation rate would be a multiple of the true value (see for further details McQuillan et al. 2013a). To minimize this problem, we compute the wavelet power spectrum of the lightcurves and we project it on the period axis, which reinforces the power of the fundamental peak and reduces the heights of the overtones (for further details about the methodology see Mathur et al. 2014a). McQuillan et al. (2013a,b, 2014) also studied the autocorrelation function of the *Kepler* time series to determine respectively rotation rates of M dwarfs, *Kepler* Objects of Interests (KOI), and around 34,000 main-sequence stars, using PDC-MAP data from Q1 to Q4 for the first study and from Q3 to Q14 for the last two. By using the autocorrelation function, they demonstrated that they were less sensitive to instrumental problems than the direct analysis of the low-frequency part of the power spectrum.

In the present study we apply two of these methods: the autocorrelation of the light curves and the study of the low-frequency part of a time-period analysis projected onto the period domain (see next subsections for more details). We also use the time-period analysis to determine whether or not the rotation period detected is due to a localised instrumental glitch in the light curve or if it is a persistent feature in time that could then be interpreted as the true stellar rotation. All these analyses are performed using PDC-MAP and KADACS time series, rebinned by a factor of four to speed up the process, and put on a regularly spaced time array (see an example in the top panels of Fig 2, corresponding to KIC 12258514). The comparison of the results obtained from different methods allows us to check the reliability of the extracted rotation period. Moreover, while most of the aforementioned works analysed a single quarter or a few of them concatenated together, we take advantage of much longer light curves from Q0 up to Q14.

3.1. Time-frequency analysis and projected power spectrum

The first study we perform to measure the surface rotation is a time-period analysis using a wavelet decomposition (Torrence & Compo 1998), improved for the low-frequency region as in Liu et al. (2007), and adapted to our asteroseismic purposes following Mathur et al. (2010b). This study allows us to track the temporal evolution of any modulation in the light curve that could be related to the rotation period and hence check if it is not due

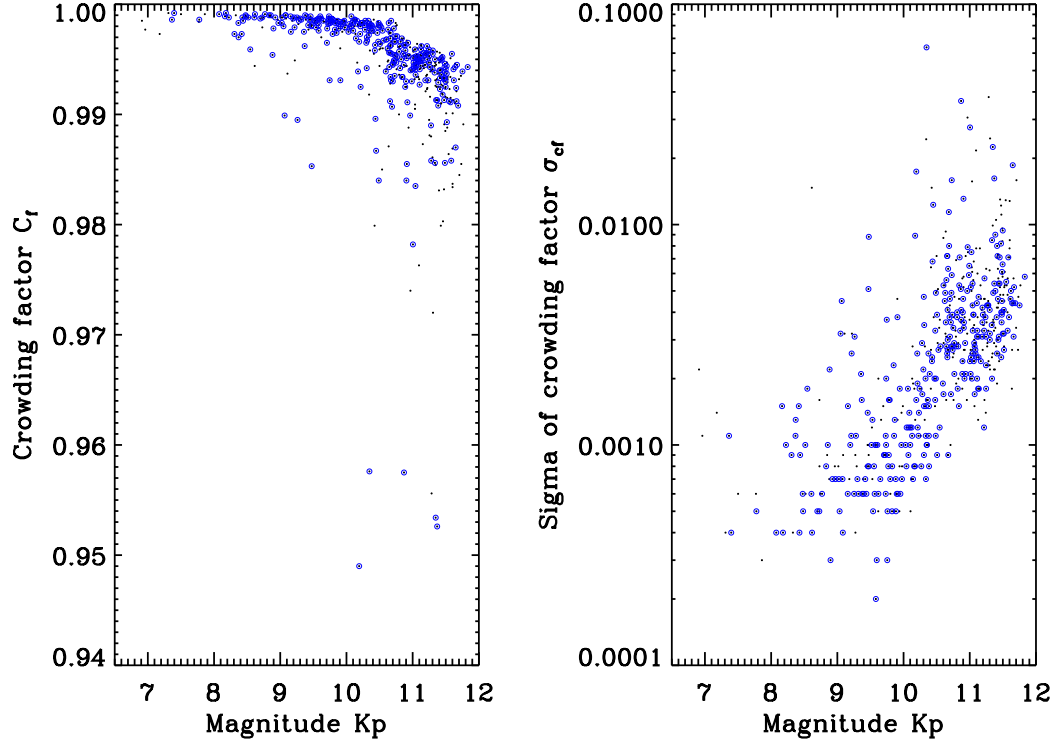


Fig. 1. Crowding factor, C_f (left panel) and sigma on the crowding factor, σ_{C_f} (right panel) for the 540 stars in the analysed sample (black dots) as a function of the *Kepler* magnitude. The 310 stars with measured P_{rot} are indicated by the blue circles.

to a sudden event in the time series (normally related to a instrumental perturbation).

We use a Morlet wavelet – which is the convolution of a sinusoid and a Gaussian function – as the mother wavelet (Goupillaud et al. 1984; Holdschneider et al. 1989). The principle of the wavelet analysis consists of computing the correlation between the mother wavelet and the data by sliding the wavelet along the time axis of the light curves for a given scale or frequency of the wavelet. Then, we probe a range of scales for the wavelet and redo the analysis. This produces the Wavelet Power Spectrum (WPS) (see for example Fig. 2, middle left panels). The red areas correspond to high power, while blue represents low power. This enables us to see if the rotation signature is present in the entire light-curve. To increase our confidence in the estimation of the rotation period, we require that at least four rotations are observed in our light curves. This is delimited by the “cone of influence” that also takes into account edge effects (black-crossed area in the middle left panels of Fig. 2).

Finally, we project the WPS along the period axis yielding the Global Wavelet Power Spectrum (GWPS, thick black line in the middle right panels of Fig. 2), which is similar to a Fourier power spectrum but with a degraded resolution. When the rotation period is well defined, the GWPS shows an almost perfect Gaussian profile. Therefore, in order to estimate the rotation period from the GWPS, we process as follows. In a first step, all the N peaks in the GWPS with periods between 0.5 and 100 days are found. Then, the GWPS is described and least-squared minimized using the combinations going from N to 1 Gaussian functions, removing iteratively the lowest peak. Finally, the fitted profile with the lowest reduced chi-squared is returned (green line in the middle right panels of Fig. 2).

The rotation period, P_{rot} , of the star is first assumed to correspond to the highest fitted peak in the GWPS. An estimate of the uncertainty –including any possible differential rotation– is given by the Half Width at Half Maximum (HWHM) of the fitted profile.

Other harmonics of the signal can also be identified and fitted. Therefore, one can verify if there are peaks with lower amplitudes that are multiples of the assumed P_{rot} , in particular, if there are multiples at higher periods that could indicate that the selected P_{rot} is the second or the third harmonic of the stellar rotation period.

3.2. Autocorrelation function of the light curve

The second analysis performed to derive P_{rot} is the autocorrelation of the light curves. This is done following a modified version of the procedure described by McQuillan et al. (2013a). For a given light curve of a total duration T and a time step δt , we compute the autocorrelation function, ACF, from 0 to $0.5 * T$ with a step δt . We then compute the power spectrum of the ACF to get the most relevant period present in the ACF. Knowing this value, we smooth the ACF with a Gaussian function of width a tenth of the selected period. This is done in order to minimize “jitter” effects in the ACF due to the presence of noise and other high-frequency effects such as stellar pulsations.

Once the ACF is smoothed, we identify the first ten maxima whose heights are above a given threshold –empirically set to 0.1–. The first of these maxima –with the shortest period– is assumed to correspond to P_{rot} . In addition, we check for the signature of a double dip or triple dip, i.e., a structure in which one or two small peaks are followed by a higher one. This shape of the

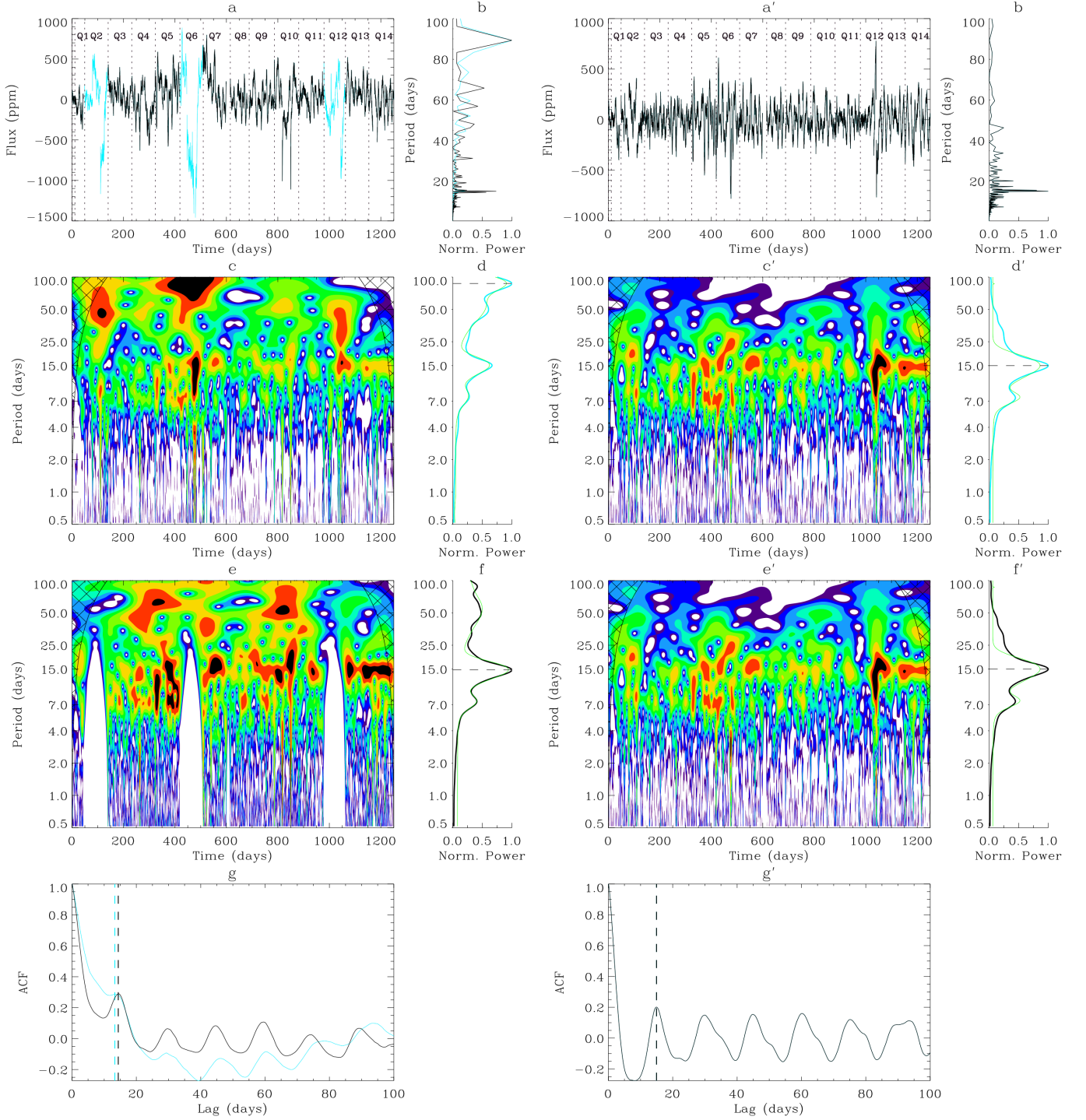


Fig. 2. Comparison of the two analyses used in this work: ACF and GWPS, applied on the two different datasets used PDC-MAP (left-hand side panels) and KADACS (right-hand side panels marked with a “prime”) for KIC 12258514. For each dataset, the plots are as follow. Top panels (a): Long-cadence *Kepler* light curves (cyan) and the quarters selected for the analysis (black), where vertical dotted lines indicate the transitions between the observing quarters. Top right panels (b): associated power density spectrum as a function of period between 0.5 and 100 days. Middle left panels (c and e): Wavelet Power Spectrum (WPS) computed using a Morlet wavelet between 0.5 and 100 days on a logarithmic scale. (c) panels correspond to the analysis of the entire light curve while in the (e) panels only the selected portions of the light curve are used in the analysis. The black-crossed area is the cone of influence corresponding to the unreliable results. Middle right panels (d and f): Global Wavelet Power Spectrum (GWPS) as a function of the period of the wavelet (thick cyan line for (d), thick black line for (f)) and the associated fit composed from several gaussian functions (thin green lines). The horizontal dashed line designates the position of the retrieved P_{rot} . Bottom panels (g): AutoCorrelation Function (ACF) of the full light curve plotted between 0 and 100 days (cyan) and using only the selected portions of the light curve (black). The vertical dashed line indicates the returned P_{rot} for the ACF analysis.

ACF can be due to the presence of several active regions on the star at different longitudes (e.g. Fig. 2 in McQuillan et al. 2013a). If such a structure is revealed repeating itself, we select as P_{rot} the highest peak of the repeated sequence in the ACF. If we do not detect any peak above the aforementioned threshold of 0.1, the star is assumed to be magnetically inactive (or having a very low inclination angle) and no P_{rot} is given. The bottom panels of Fig. 2 shows an example of the ACF (black) and the smoothed version of the ACF (blue), which in this particular case are indistinguishable. The peak around 15 days –marked by the vertical dashed line– corresponds to the extracted rotation period.

Even if the PDC-MAP light curve suffers from a noticeable jump and other instrumental instabilities, the autocorrelation function managed –for both datasets– to extract the correct rotation period while the analysis of the GWPS failed when PDC-MAP data were used.

3.3. Extracting stellar rotation periods

While these methods are a relatively robust means to derive the rotation period P_{rot} , it is important to remember that the *Kepler* lightcurves are divided into ~ 90 days-long quarters and that the data are interrupted every month when the satellite faces the Earth to download the recorded data. Thus, these two periodicities (~ 30 and ~ 90 days) often appear in the *Kepler* lightcurves and possibly in the results of the autocorrelation function analysis. For this reason, a comparison between the two sets of light curves and a visual check of the results are needed to ascertain the surface rotation period derived.

From the four values obtained using the two sets of data –PDC-MAP and KADACS– and the two analysis methods –GWPS and ACF– we extract a reliable surface rotation period. To do so, we compare the four values and check if they agree within 20%. If at least two results from two different sets agree within this value, we consider that this period is the rotation period of the star. We define P_{rot} and its uncertainty as the centre and the HWHM of the fit of the corresponding peak in the GWPS of the KADACS data set. We choose this solution because it is difficult to derive a reliable uncertainty on the rotation period from the ACF method, as pointed out by McQuillan et al. (2013a), and because we have a complete knowledge of all the corrections of the KADACS light curves.

After this first automatic comparison, we visually check every light curve to verify that problems in the data do not prevent the automatic estimation of P_{rot} . For some stars, the returned P_{rot} clearly comes from a common artifact in both sets of data, in which case we classify this period as not reliable. For some other stars, the light curves are clearly showing a rotational modulation but a glitch in one of the two sets prevents the comparison of the four results to work. In this case, we add these stars to the list of rotators, with a P_{rot} coming from the fit of the GWPS of the most stable of the two light curves, as indicated in Table 2. Finally, we separate the stars that show absolutely no rotation modulation from the ones that are just too noisy or unstable to get a reliable result. It is also during this visual inspection that we find the stars for which a filter limit of 30 days is too small and re-filter them with a filter limit of 100 days for the KADACS set before re-applying the same methodology to the new light curves.

From the 540 stars of our sample, we found 321 for which we can determine a robust surface modulation period. Our sample can then be divided into 4 different groups. The first group is composed of the 310 normal stars (i.e. non binaries) for which we derive a surface rotation period (see Table 2). The second

Table 1. Number of stars belonging to the different categories returned.

Category	Total	Binaries	KOI
Whole sample	540	15	15
Period detected	321	11	12
No sign of rotation	6	0	1
No reliable P_{rot}	213	4	2

group is composed of the 15 binaries or multiple stars in our sample. These 15 stars are either eclipsing binaries from the *Kepler* Eclipsing Binary Catalog (<http://keplerebs.villanova.edu>, Kirk et al 2013, in preparation) for which our method returns the orbital period, double-lined spectroscopic binaries from (Griffin 2007) and Thygesen et al. (2014), stars flagged as *Double or multiple star* or *Star in double system* in the SIMBAD database (<http://simbad.u-strasbg.fr/simbad/>) or the previously mentioned possible seismic binary or star polluted by a nearby red giant – KIC 7938112 – for which our method detects the low-frequencies solar-like oscillations. The results for these multiple stars are regrouped in Table 3. We have also found 6 stars showing no signs of rotation in their lightcurve (third group, see Table 4) and 213 stars for which the lightcurves are too noisy to derive a reliable result (fourth group). This repartition is summarized in Table 1. It is important to notice that amongst the stars listed in Table 2, there are 12 KOIs. For each of these stars, we check that the returned rotation period is not due to the transiting planet candidate. In Fig. 3 are shown all stars for which a P_{rot} was derived and a large spacing is available from Chaplin et al. (2014).

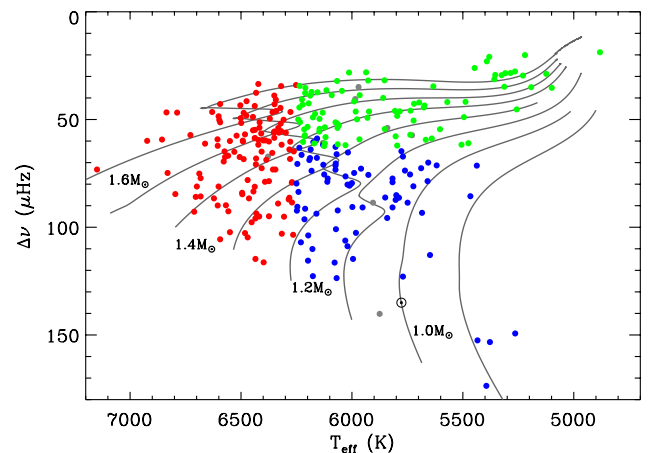


Fig. 3. Modified H.-R. diagram ($\Delta\nu$ vs T_{eff}) showing the Sun and the 297 stars for which the rotation period, P_{rot} , was successfully measured and a large frequency spacing is available from Chaplin et al. (2014). Hot stars are shown in red and defined as having $T_{\text{eff}} > 6250$. Dwarfs ($T_{\text{eff}} \leq 6250$ and $\log g > 4.0$) are shown in blue, and subgiants ($T_{\text{eff}} \leq 6250$ and $\log g \leq 4.0$) in green. Effective temperatures are taken from Pinsonneault et al. (2011). The stars plotted in grey correspond to those for which only the effective temperatures from Huber et al. (2014) are available. Evolution tracks, computed with the ASTEC code (Christensen-Dalsgaard 2008), are shown for a range of masses at solar composition ($Z_{\odot} = 0.0246$).

These stars are divided into three groups based on the stellar parameters in Chaplin et al. (2014): cool main-sequence dwarfs (blue, $T_{\text{eff}} \leq 6250$ K, $\log g > 4.0$), hot stars (red, $T_{\text{eff}} > 6250$ K), and subgiants (green, $T_{\text{eff}} \leq 6250$ K, $\log g \leq 4.0$). To have an homogeneous set of temperatures we use those derived by Pinsonneault et al. (2011) who performed a recalibration of the KIC photometry in the SDSS *griz* filters using YREC models.

The repartition of reliable P_{rot} can be seen in the form of a histogram in Fig 4. As it will be discussed in Sect. 5.1, hot stars rotate in general faster than cool main-sequence dwarfs, while the expansion of stars as they evolve on the subgiant branch leads to long rotation periods.

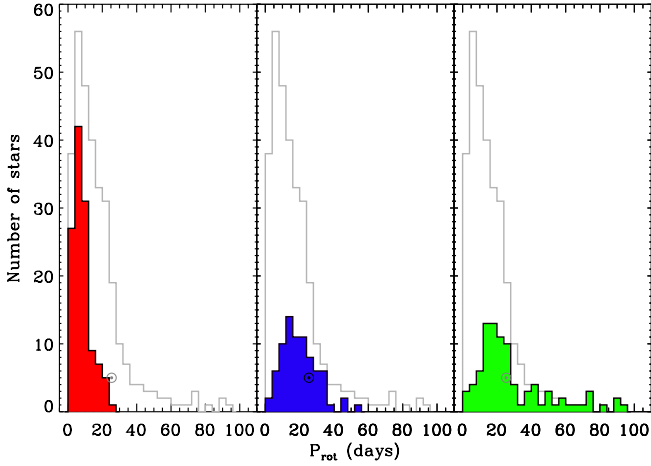


Fig. 4. Histograms of the extracted surface rotation periods, P_{rot} , for the full sample (grey), hot (red), dwarf (blue), and subgiant stars (green) as defined in Fig. 3. For comparison with our sample of dwarfs, the solar rotational rate (25.4 days) is represented in black in the central panel at an arbitrary Y axis of 5. In the left and right panels, the Sun is plotted in grey as a guidance for the eyes only.

4. Extracting the photometric magnetic activity level

Using CoRoT observations of HD 49933, García et al. (2010) demonstrated that the presence of spots and magnetic features on the surface of a star followed the internal magnetic activity changes deduced from the analysis of the acoustic modes. A global index of stellar photometric variability, S_{ph} , was defined from the standard deviation of the whole light curve. In the case of the Sun, the comparison of S_{ph} with a well established magnetic activity proxy, the 10.7 radio flux, demonstrated that S_{ph} is a good indicator of the surface magnetic activity of the Sun (García et al. 2013b). Basri et al. (2011) also defined a photometric variability index, called the *range*: $R_{var}(t_{len})$, to characterize the variability of the *Kepler* targets at different time scales. This index, calculated by taking the flux included between 5% and 95% of the span in brightness, can however underestimate the variability level of very active stars. Basri et al. (2013) calculated R_{var} for the exoplanet targets Q9 timeseries of about 90 days, which were reduced using the PDC-MAP pipeline. R_{var} was determined as the median value of segments of a given length, $t_{len} = 30$ days. This length was chosen because it is close

to the solar rotation period. However, the variability in the light curves can have different origins such as stellar pulsations, convection, or the presence of spots on the surface of the star, which are linked to the rotation period. For these reasons, and in order to specifically study stellar magnetic activity, the rotation period of the star needs to be taken into account in the calculation of the magnetic activity index. In this way, most of the variability should be related to the magnetism (spots) and not to the other sources of variability. However, it should be noted that the stellar inclination along the line of sight affects the observed value of the variability index, if we assume that the stellar variability in solar-type stars is dominated by contributions from active latitudes like for the Sun. Consequently, an intrinsically active star observed at a low angle of inclination may present a moderate-to-low variability index.

Helioseismology has proven that the surface magnetic activity is related to an inner dynamo process linked to the turbulence and the differential rotation between the envelope and the base of the convective zone. The rotation period is thus a key parameter to understand stellar magnetism. Moreover, when defining a stellar magnetic variability index for a large sample of stars it should be able to take into account any temporal variations of the activity, with periods of lower and higher activity, given the long time-series provided by the *Kepler* mission. The stellar variability indices determined so far (García et al. 2010; Basri et al. 2011, 2013) do not use the rotational period as input. In this section, we aim to determine a global magnetic activity index linked to the rotation period, which can also provide the possibility to study the temporal evolution of the stellar activity. To do so, the Q0 to Q14 *Kepler* light curves –for a total of over 1200 days– are divided into sub-series of $k \times P_{\text{rot}}$, where P_{rot} is the rotational period of a given star, as measured in Sec. 3, and k an integer. For each individual sub-series, the standard deviation $S_{ph,k}$ of the non-zero values is calculated. The non-zero values include any quarter which was not observed for a given star or removed as being identified as *bad* (see Sec. 2). Moreover, a given sub-series is used only if the length of the sub-series is at least 2.5 times P_{rot} in order to avoid the introduction of any bias between sub-series. The magnitude correction of the photon noise from Jenkins et al. (2010) is then applied to the $S_{ph,k}$.

As an example, Fig. 5 shows the light curve of the star KIC 6448798 from Q0 to Q14 spanning more than 1200 days (top left panel). The rotational period measured for this star is $P_{\text{rot}} = 6.44 \pm 0.56$ days. The following panels show the evolution of the magnetic index $S_{ph,k}$ calculated for different values of the factor k (1, 3, 5, 10, and 30) as a function of time. The black dashed line represents the value of the standard deviation over the entire time series, S_{ph} , while the red dot-dashed line corresponds to the mean value of the standard deviations, $\langle S_{ph,k} \rangle$, calculated for each k . The mean value instead of the median value is used as the median can underestimate the activity level if there is an on-going magnetic activity cycle. As shown in Mathur et al. (Submitted), the value of $\langle S_{ph,k} \rangle$ is slightly smaller than S_{ph} , and the difference reaches a minimum for a given value of k . They showed that a value of $5 \times P_{\text{rot}}$ reasonably describes the magnetic temporal evolution of stars as well as to give a correct value of global activity index. This was also well demonstrated in the case of the Sun with the photometric VIRGO/SPM observations. Such photometric magnetic activity level was recently used by García et al. (2014) in the study of KIC 8561221, and for a sample of a few dozens of F (Mathur et al. 2014a) and M stars (Mathur et al. submitted).

Figure 6 shows the distribution of $\langle S_{ph,k} \rangle$ for $5 \times P_{\text{rot}}$ for the 310 stars for which a rotation period P_{rot} was measured (Sec. 3).

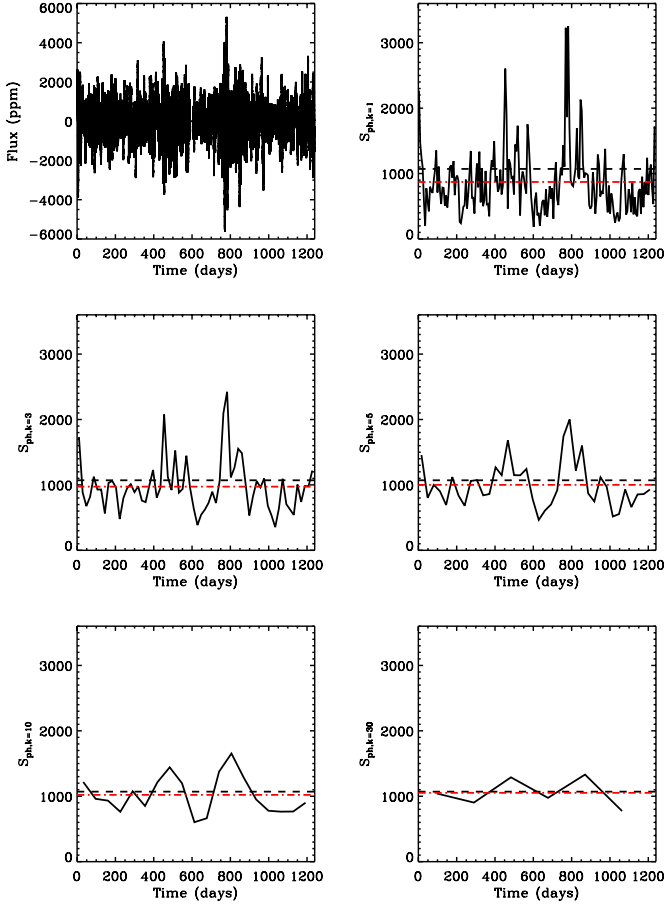


Fig. 5. Light curve of the solar-like pulsating star KIC 6448798 observed by *Kepler* from Q0 to Q14 (top left panel). From top right to bottom right panel, photometric magnetic activity index, $S_{ph,k}$, calculated using sub-series of size $k \times P_{rot}$ with $k = 1, 3, 5, 10$, and 30 . The black dashed line represents the global magnetic index, S_{ph} , and the red dot-dashed line corresponds to the mean magnetic index, $S_{ph,k}$.

The figure is color-coded following the three categories defined in the previous section: hot, dwarfs, and subgiant stars. The distribution of the activity levels appear to be similar for the three categories of stars we have measured. Most of the stars in the sample have a $\langle S_{ph,k=5} \rangle$ located between the minimum and maximum solar magnetic activity of 89 ± 1.5 and 258.5 ± 3.5 ppm, respectively (Mathur et al. 2014a). In particular, from a total of 78 dwarf stars, 48 of them (61.5%) lie between the limits of the solar activity, 19 (24.4%) are more active, and 11 (14.1%) are less active. For the hot stars, the distribution is skewed toward higher values than the dwarfs and the subgiants.

To place this study in a wider context, it is important to recall that the sample of stars used in this work have been chosen because pulsations have been measured. Therefore, because magnetic activity inhibits stellar pulsations (e.g. García et al. 2010; Chaplin et al. 2011), and the amplitudes of the modes increase with age, our set of stars is biased towards aged stars (see Fig.3) with moderate magnetic activity.

The variability index proposed by Basri et al. (2013) is calculated on segments of 30 days of data, which naturally introduces a bias towards slow rotators. In order to estimate that bias,

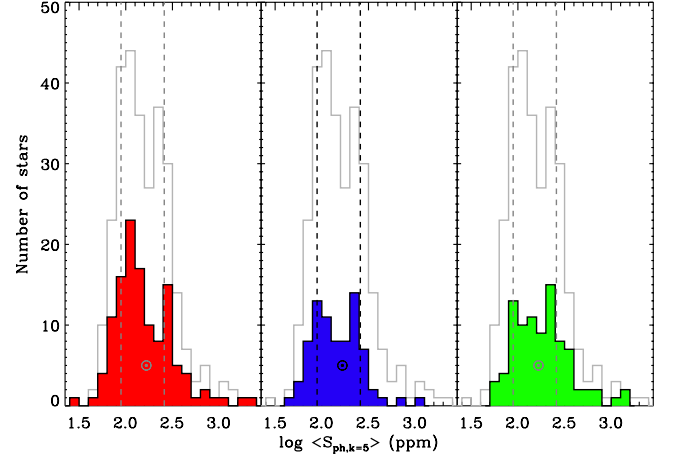


Fig. 6. Histograms of the extracted photometric magnetic activity level, $\log\langle S_{ph,k=5} \rangle$, for the full sample of stars for which we have retrieved a P_{rot} (grey), hot (red), dwarf (blue), and subgiant stars (green) as defined in Fig. 3. For reference, the activity of the Sun (166.1 ± 2.6 ppm) is also shown. The vertical dashed lines enclose the solar magnetic-activity range (from 89 to 258.5 ppm). The solar values are color coded as in Fig. 4.

we calculated the *range*, $R_{var}(30 \text{ days})$, as in Basri et al. (2013) for the 310 stars. Figure 7 shows the ratio between the magnetic activity level, $\langle S_{ph,k=5} \rangle$, and $R_{var}(30 \text{ days})$ as a function of the rotation period P_{rot} . A bias is clearly introduced for stars with a slower rotation period, $R_{var}(30 \text{ days})$ underestimating their activity level by about 30% compared to stars with a fast rotation period within the same sample.

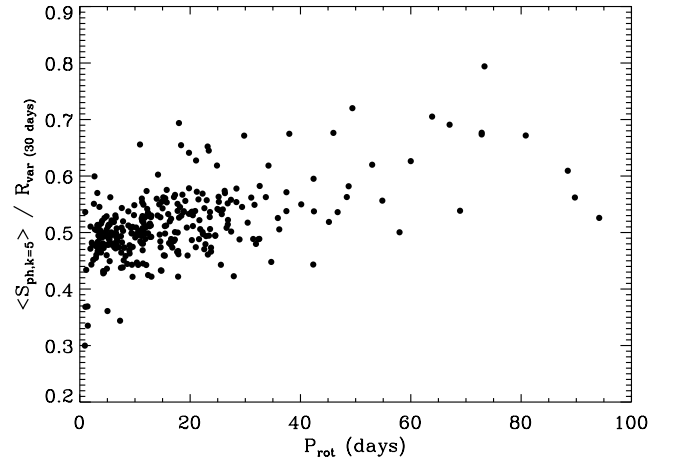


Fig. 7. Ratio between the measured photometric magnetic activity level, $\langle S_{ph,k=5} \rangle$, and the *range*, $R_{var}(30 \text{ days})$ (Basri et al., 2013) as a function of the rotation period P_{rot} for the 310 solar-like pulsating stars observed by *Kepler*.

5. Discussion

We can first compare our results with those obtained by McQuillan et al. (2014) who determined the P_{rot} of many main-sequence stars – with no binaries – by studying the autocorrelation function of their PDC lightcurves. Their results were divided into two categories: “Periodic”, when they had a reliable P_{rot} , and “Non Periodic”, when no P_{rot} could be obtained or when they found that the obtained P_{rot} was not reliable. From our sample of reliable P_{rot} , we find 114 stars in common with their “Periodic” sample. For these stars, both results are in good agreement within one sigma with one exception – KIC 4931390 – for which they derive a very small period of 0.57 days while we find a much longer rotation period of 7.45 days. We also find 155 stars for which we derive a reliable P_{rot} , while they classified them as “Non Periodic” sample. Among these 155 stars, their method still derives a non-reliable rotation period for 129 stars. For them, the P_{rot} of 102 stars are in agreement with our results within 2σ , 17 stars agree with twice our P_{rot} , and 1 star agrees with half our P_{rot} . All of them are within 2σ . This leaves only 9 stars for which the two analyses are not in agreement. As our methodology includes a visual inspection of every single target, we can say that the periods we derive for these stars are robust. Moreover, when we do not derive a rotation period for a star, no rotation period is obtained by McQuillan et al. (2014).

We can then compare our results with the ones obtained by Karoff et al. (2013) who determined the rotational periods, P_{rot} , from the periodograms of the PDC *Kepler* light curves, as well as the chromospheric activity S indexes from spectroscopic observations for a small subset of the targets analysed in this paper. In this sub-sample, Karoff et al. (2013) measured P_{rot} for 10 stars. In 8 stars both results agree within 1σ . For KIC 8694723, we were unable to extract a reliable P_{rot} (see Table 4), while Karoff et al. (2013) measured a rotation period of 7.5 ± 0.2 days. Finally, our results disagree in KIC 4914923. Indeed, we find a rotation period of 20.49 ± 2.82 days, while they found 8.1 ± 0.4 days. However, Karoff et al. (2013) limited their analysis of the periodograms between 0 and 20 days. Thus, any P_{rot} longer than 20 days could not be detected. A close visual inspection of our GWPS and ACF analyses from both PDC-MAP and KADACS datasets show a prominent and clear signature of the rotation around 20 days. However, a smaller peak around 8 days is also visible, but its signature is much fainter and could be due to the third harmonic of P_{rot} .

Among the stars with measured reliable periods we have found 15 KOIs –with 3 confirmed systems and 1 false positive– for which in two of them the extracted P_{rot} is a multiple of the transit period. All of them are single systems to the best of our knowledge. By studying P_{rot} as a function of the orbital period of the innermost planet, we found that there are no close-in planets around fast rotators in this small sample of asteroseismic targets as pointed out by McQuillan et al. (2013b). The study of the KOI light curves requires a specific analysis in order to properly remove the transit signature without affecting the rotation modulation.

5.1. Gyrochronology and age-rotation relations in the context of stellar populations

This sample has the potential to provide calibration points for empirical gyrochronology relationships. We examine the relationship between surface rotation periods and ages by combining both the periods provided in this work and the ages from Metcalfe et al. (2014) and Chaplin et al. (2014). It is important

to consider our theoretical expectations regarding the relationship between rotation period and age. Cool main-sequence stars undergo magnetic braking and spin down as a function of time (Skumanich 1972), and should therefore display a correlation between period and age. Hot stars ($T_{\text{eff}} > 6250$ K), however, should not, since their thin convective envelopes and presumably weak dynamos result in very little magnetic braking. Subgiants –whose rotation rates are modified by the addition of substantial envelope expansion– should display a relationship between period and age, but of a different form than that observed on the main sequence. We have therefore divided our sample into three groups based on the stellar parameters in Chaplin et al. (2014): cool main sequence dwarfs (blue, $T_{\text{eff}} < 6250$ K, $\log g > 4.0$), hot stars (red, $T_{\text{eff}} > 6250$ K), and subgiants (green, $T_{\text{eff}} > 6250$ K, $\log g < 4.0$).

Shown in Fig. 8 are ages from Chaplin et al. (2014) plotted against the P_{rot} from this work. These three subsets populate the period-age diagram in a manner consistent with the theoretical predictions of van Saders & Pinsonneault (2013), and demonstrate that care must be taken in interpreting the rotation periods of stars in such a sample. The curves represent the period-age relationships from Mamajek & Hillenbrand (2008) for B-V = 0.5 and B-V = 0.9, corresponding to roughly 0.8 and 1.2 M_{\odot} respectively. Stars within this mass range that obey the gyrochronology relationships should fall between these two curves, and indeed the cool star sample displays this behavior. Hot stars, however, do not: a large fraction of the hot stars lie at systematically faster rotation periods and older ages than gyrochronology would have predicted. These stars do not spin down as a function of time due to weak magnetized stellar winds, and thus do not have a strong relationship between period and age. Likewise, many of the subgiants fall outside of the gyrochronological period-age relationships, again because their rotational history is different than that of a cool main-sequence dwarf. They expand on the subgiant branch and continue to lose angular momentum through winds, and as a result, can populate the young, slowly rotating quadrant of this diagram. One should also note that certain period regimes (~ 20 days, for example) contain a mixture of dwarfs, hot stars, and subgiants, all of which have different relationships between period and age. We can, however, select a sample of dwarfs for which we expect to see a standard period-age relationship: stars in the dwarf subset, restricted to objects with periods of 5 days or longer – to avoid potential contamination from synchronized binaries, or very young objects for which the period-age relationships are less reliable (see Epstein & Pinsonneault 2014) – and which have precise ages derived from the seismic frequency spectra. We thus take 12 stars analysed by Metcalfe et al. (2014): KIC 3427720, KIC 6116048, KIC 7871531, KIC 8006161, KIC 8228742, KIC 9098294, KIC 9139151, KIC 9955598, KIC 10454113, KIC 10644253, KIC 11244118, and KIC 12258514; as well as 3 more stars from Mathur et al. (2012): KIC 3656476, KIC 5184732, and KIC 7680114. If we follow Metcalfe et al. (2014) and Karoff et al. (2013) and simply fit a line to the Sun –considering a P_{rot} of 25.4 days and a dummy error in period of 1%, and an age of 4.570 ± 0.007 years (Bahcall et al. 1995)– and the above mentioned 15 stars in $\log(t) - \log(P_{\text{rot}})$ space (see Fig. 9), we find

$$\log P_{\text{rot}} = (0.52 \pm 0.09) \log(t) + (0.99 \pm 0.06), \quad (1)$$

where P_{rot} in days, and t in Gyrs. This slope is in good agreement with published slopes, n , in the literature: the original Skumanich (1972) relation with $n = 0.51$, Barnes (2007) with $n = 0.5189 \pm 0.0070$, and Mamajek & Hillenbrand (2008) with $n = 0.566 \pm 0.008$. It is less steep than the $n = 0.75 \pm 0.03$ value

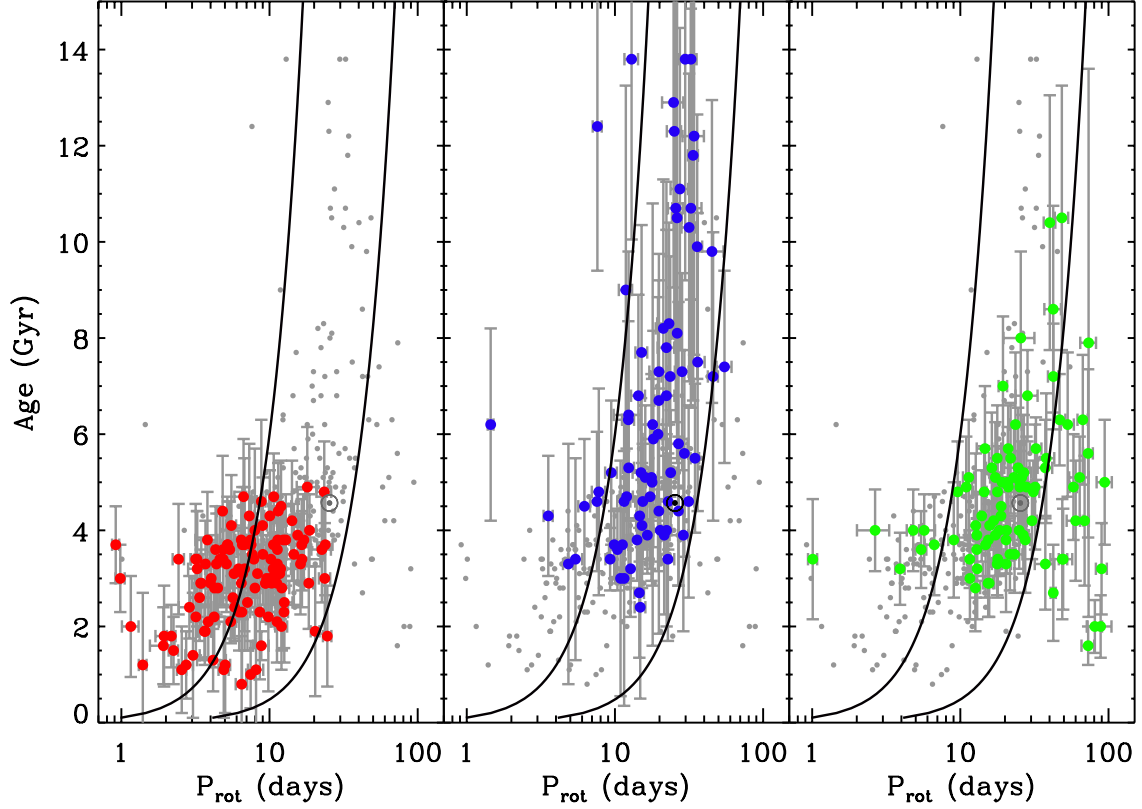


Fig. 8. Rotation periods measured in this work as a function of ages taken from Chaplin et al. (2014). Stars have been divided in hot (red), dwarfs (blue) and subgiants (green) as defined in Fig. 3. The solid black curves represent the period-age relationships from Mamajek & Hillenbrand (2008), plotted for $B-V = 0.5$ and $B-V = 0.9$, corresponding to late F to early K spectral types. As expected, only the cool dwarfs fall consistently between the two curves; the hot stars and subgiants do not obey these same period-age relationships. The position of the Sun in the diagram is indicated by the \odot symbol and color coded as in Fig. 4.

derived in Metcalfe et al. (2014); we believe this is the result of our careful sample selection, which here includes only the cool, unevolved stars for which gyrochronology is valid. From the Mamajek & Hillenbrand (2008) calibration, one expects the intercept of the period-age relation for the typical star in our sample with $B-V = +0.58$ ($\sim 1.05 M_{\odot}$) to be 0.96 ± 0.05 , or 1.00 ± 0.04 from the Barnes calibration, both of which are consistent with our result. In comparison, when the full sample with Chaplin et al. (2014) ages is fit, including all evolved, dwarf, and hot stars, the power-law slope of the relation is ~ 2.2 : an unreasonable value, derived from an unreasonably mixed population of stars. Further, in-depth analysis of the gyrochronological consistency and value of this dataset is reserved for later papers; for now, it is sufficient to emphasize the fact that stellar populations and sample selection are important when deriving period-age relationships.

5.2. Age-rotation-activity relations

Figure 10 shows in a log-log scale the photometric magnitudes measured. The three groups of stars defined in Sec. 5.1 are represented on separate panels with the same color coding as used in Fig. 8. The solar value is also represented, while the horizontal dashed lines represent the corresponding solar magnetic activity level at minimum and maximum of the 11-year solar cycle.

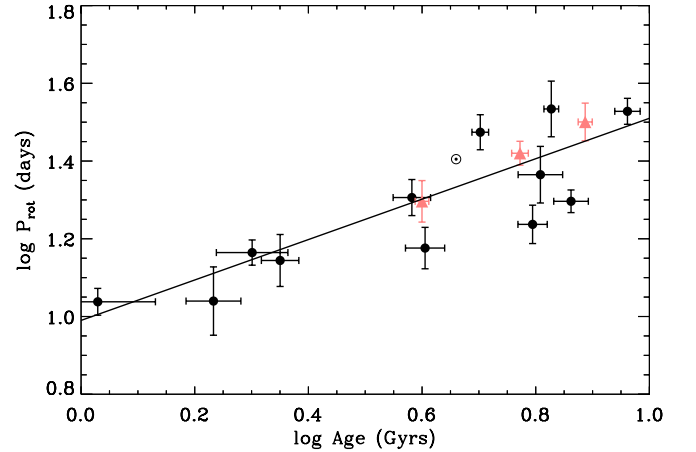


Fig. 9. Rotation periods, P_{rot} , as a function of the asteroseismic ages in a log-log space. These ages are given by Metcalfe et al. (2014) for 12 stars and Mathur et al. (2012) for 3 other stars. The solid line corresponds to a linear fit including the Sun considering it has a rotation period of 25.4 days and an age of 4.57 Gyr.

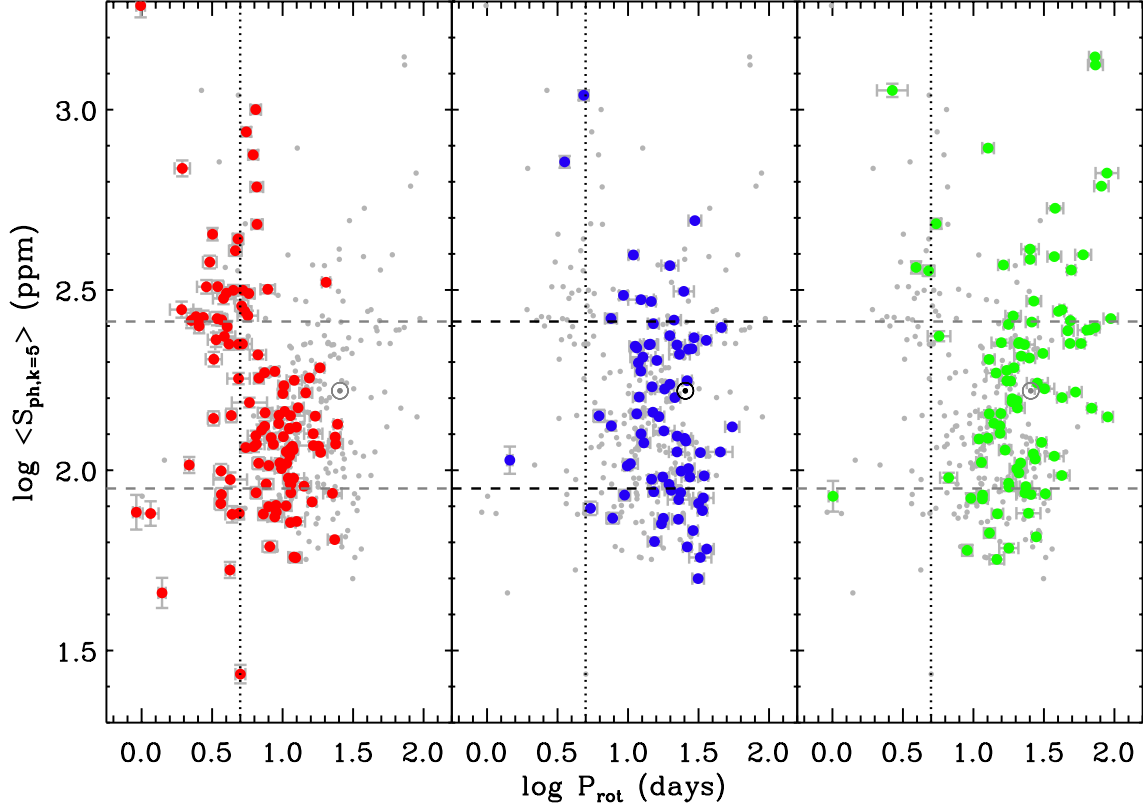


Fig. 10. Photometric magnetic activity level, $\langle S_{ph,k=5} \rangle$, as a function of the rotation period, P_{rot} , for the 310 solar-like pulsating stars observed by *Kepler* for which the rotation period was successfully measured (grey). Stars have been divided in hot (red), dwarf (blue), and subgiants (green) as defined in Fig. 3. The vertical black dotted lines mark the limit of $P_{rot} = 5$ days. The position of the Sun, $\langle S_{ph,k=5} \rangle = 166.1 \pm 2.6$ ppm and $P_{rot} = 25.4$ days is indicated. The top and bottom dashed horizontal lines represent the corresponding solar magnetic activity level at maximum and minimum of the 11-year solar cycle respectively. The solar values are color coded as in Fig. 4.

cle (Mathur et al. 2014a). We want to note that some of the stars with a large $\langle S_{ph,k=5} \rangle$ and a low P_{rot} could be possible multiple systems as they have very stable ACFs.

For each subsample, we look for correlations between $\log P_{rot}$ and $\log S_{ph,k=5}$. We first consider stars with $P_{rot} > 5$ d for the same reasons as explained in Sec. 5.1. For hot stars, cool dwarf and subgiants, the correlations are -31%, -15%, and 43%, respectively. By restricting the sample to $P_{rot} > 10$ d, the correlations become 12%, -27%, 49%. The correlation are weak or very weak. For hot stars, the slight anticorrelation in the first sample was only due to a few stars with high $S_{ph,k=5}$ and P_{rot} between 5 and 10 days, well visible on Fig. 11. Concerning the sample of dwarfs, the found anticorrelation is hardly significant. The most significant signature is the correlation found for the subgiant sample. This correlation leads to the following relation:

$$\log P_{rot} = (0.77 \pm 0.04 \pm 0.15) \log(\langle S_{ph,k=5} \rangle) - (0.32 \pm 0.08 \pm 0.30). \quad (2)$$

This relation corresponds to the principal component of the sample (as defined in a Principal component analysis). The first error bars are the statistical errors. We restrict the analysis to $P_{rot} > 10$ d to minimize the risk of contamination by multiple systems. To understand this loose correlation, we need to note that the dispersion of $S_{ph,k=5}$ in the sample is similar to the range spanned by the Sun between a minimum and a maxi-

mum of its activity. As a consequence, $S_{ph,k=5}$ do probably not reflect the mean activity level of the stars. This additional dispersion naturally introduces decorrelation. Observing stars during years would probably smear out this effect. We also note that the statistical error bars for each point is significantly smaller than this dispersion. The rms dispersion of $S_{ph,k=5}$ due to the activity change is $\sigma \sim 0.15$. Hence, we compute additional error bars, the second ones in Eq. 2, through Monte Carlo simulations.

To go further in the investigation of the rotation-activity relation it would be necessary to separate stars by their masses and metallicities to properly separate those effects from the general trend. This is out of the scope of this paper and will be done in the near future.

Figure 11 shows the age-activity relation for the set of stars with measured P_{rot} , taking the ages from Chaplin et al. (2014). Hot stars are represented in red, dwarfs in blue, and subgiants in green. In previous works, the age-activity relation derived from the chromospheric S-index shows a rapid decay of chromospheric activity up to 2 Gyr, and no decay above that (Pace 2013). Unfortunately, most of the stars in our sample are concentrated in a bulk between 3 and 5 Gyr, and only $\sim 4\%$ have an age less than 2 Gyr, which makes it difficult the comparisons with Pace (2013)'s observations. Nevertheless, it is worth noting that while the photometric magnetic activity levels $\langle S_{ph,k=5} \rangle$ are mostly in the range between 60 and 300 ppm, some of the

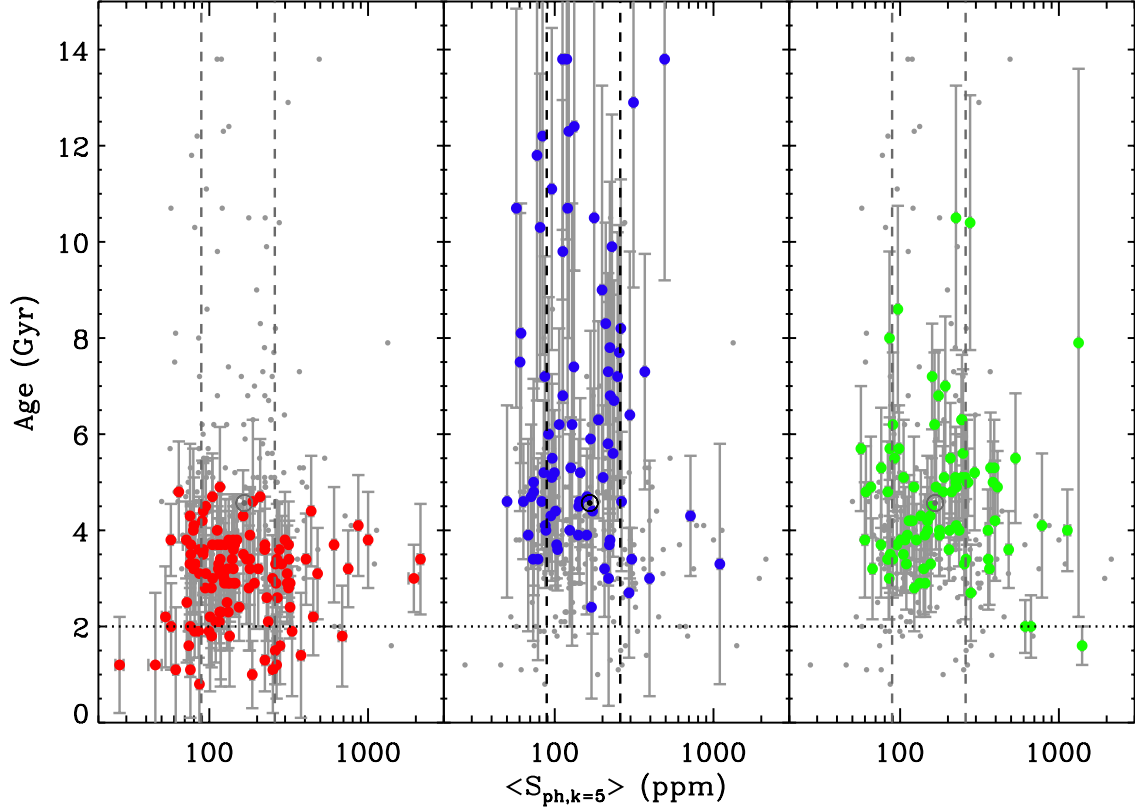


Fig. 11. Photometric magnetic activity level, $\langle S_{ph,k=5} \rangle$, as a function of ages (in grey) taken from Chaplin et al. (2014). Stars have been divided in hot (red), dwarf (blue), and subgiants (green) as defined in Fig. 3. Only stars with $P_{\text{rot}} \geq 5$ days are shown. Due to the size of the error bars, they are only plotted for each category of stars. The solar value of $\langle S_{ph,k=5} \rangle = 166.1 \pm 2.6$ ppm for an age of 4.57 Gyr is represented with the solar symbol and the same color code as in Fig. 4. The left and right dashed vertical lines correspond to the solar magnetic activity level at minimum and maximum of the 11-year solar cycle respectively. The horizontal dotted lines mark the 2 Gyr limit.

hot stars and subgiants show high activity levels around 3 Gyr and younger. On the contrary, these high activity levels are not observed in dwarf stars. This could be a selection bias because our stars were selected because they had acoustic modes and we know that activity reduces their amplitudes (García et al. 2010; Chaplin et al. 2011; Campante et al. 2014). Nevertheless, hot stars and subgiants with high activity levels younger than 3 Gyr could belong to the stars located at the ending part of the activity decay observed by Pace (2013). Moreover, the stellar inclination angle has a direct impact on the determination of the photometric magnetic activity levels. For future works, it will be important to study the relation between the magnetic levels and the stellar inclination angle.

6. Conclusions

In this work we have analysed the homogeneous set of 540 main-sequence and subgiant pulsating stars presented in Chaplin et al. (2014) and we have extracted reliable surface rotation periods and photometric activity indexes for 310 stars. To do so, we have combined two detection methods (GWPS and ACF) with two ways of preparing the light curves (PDC-MAP and KADACS). Special care has been taken to properly identify all the binaries in the sample in the bibliography.

These stars have been divided into three different categories, hot stars ($T_{\text{eff}} > 6250$ K), cool main-sequence dwarfs ($T_{\text{eff}} \leq 6250$ K, $\log g > 4.0$), and subgiants (green, $T_{\text{eff}} \leq 6250$ K, $\log g \leq 4.0$). As expected, the hotter stars spin faster than the cool main-sequence dwarfs because their thin convective envelopes and presumably weak dynamos result in very little magnetic braking. Subgiants can have periods of ~ 10 -100 days, depending on the main-sequence temperature and degree of expansion that the star has undergone on the subgiant branch.

To properly investigate gyrochronology relations, we have studied a set of cool dwarfs in which we have very precise age estimates from the detailed analysis of individual frequencies that matches those provided by evolutionary models from Metcalfe et al. (2014) and Mathur et al. (2012). The simple fit of a line in the $\log(t) - \log(P_{\text{rot}})$ space provides a slope $n = 0.51 \pm 0.06$ and an intercept of 0.98 ± 0.09 which are in very good agreement with literature gyrochronology calibrations.

In our sample of rotating stars we have 15 KOIs. We failed to find any close-in planet around fast rotating stars, confirming the results obtained by McQuillan et al. (2013b).

We have also studied age-rotation-activity relations and we found that the photometric magnetic activity $\langle S_{ph,k=5} \rangle$ for many solar-like pulsating stars in our sample is similar to that of the Sun during the magnetic activity cycle. Indeed, 61.5% of the dwarfs have comparable values to the Sun. Because we do not

have information on the stellar inclination axis, part of the dispersion in $\langle S_{ph,k=5} \rangle$ could be due to some degeneracy in this index as a function of the stellar inclination angle. This point will be verified in a future work when stellar inclination angles will be determined for the bulk of these stars. Moreover, this dispersion is similar to the variation of the solar $\langle S_{ph,k=5} \rangle$ during a solar magnetic activity cycle. Thus, long-term variabilities certainly contribute to spread the obtained magnetic indexes. Correlations between rotation and activity are weak, probably due to the large dispersion in $\langle S_{ph,k=5} \rangle$, nevertheless a direct correlation between $\langle S_{ph,k=5} \rangle$ and P_{rot} has been found for subgiants.

For the age-activity relation we have also found a weak correlation for the same reasons than in the activity-rotation case. Moreover, our sample is mostly composed of stars in the 3 to 5 Gyr range where previous works based on chromospheric activity show no significant variation. Only 4% of our stars are younger than 2 Gyr were most of the variation of the activity with age is expected.

Future work will look in detail at the behaviour of the gyrochronology relations at late times. Our work here highlights the importance of stellar populations in the interpretation of the rotation periods.

Acknowledgements. The authors wish to thank the entire *Kepler* team, without whom these results would not be possible. Funding for this Discovery mission is provided by NASA's Science Mission Directorate. We also thank all funding councils and agencies that have supported the activities of KASC Working Group 1, as well as the International Space Science Institute (ISSI). This research was supported in part by the National Science Foundation under Grant No. NSF PHY05-51164. The research leading to these results has received funding from the European Community's Seventh Framework Programme (FP7/2007-2013) under grant agreement no. 312844 (SPACEINN), under grant agreement no. 269194 (IRSES/ASK), under the ERC grant agreement no. 227224 (PROSPERITY), and from the Research Council of the KU Leuven under grant agreement GOA/2013/012. SB is supported by the Foundation for Fundamental Research on Matter (FOM), which is part of the Netherlands Organisation for Scientific Research (NWO). DS, RAG, SM, and TC received funding from the CNES GOLF and CoRoT grants at CEA. RAG also acknowledges the support of the French ANR under the grant IDEE. The Danish National Research Foundation (Grant agreement no.: DNRF106). The research is supported by the ASTERISK project (ASTERoseismic Investigations with SONG and *Kepler*) funded by the European Research Council (Grant agreement no.: 267864). MBN acknowledges research funding by Deutsche Forschungsgemeinschaft (DFG) under grant SFB 963/1 "Astrophysical flow instabilities and turbulence" (Project A18). This research has made use of the SIMBAD database, operated at CDS, Strasbourg, France.

References

- Appourchaux, T., Chaplin, W. J., García, R. A., et al. 2012, *A&A*, 543, A54
- Bahcall, J. N., Pinsonneault, M. H., & Wasserburg, G. J. 1995, *Reviews of Modern Physics*, 67, 781
- Ballot, J., Gizon, L., Samadi, R., et al. 2011, *A&A*, 530, A97
- Barban, C., Deheuvels, S., Baudin, F., et al. 2009, *A&A*, 506, 51
- Barnes, S. A. 2007, *ApJ*, 669, 1167
- Barnes, S. A. 2009, in *IAU Symposium*, Vol. 258, IAU Symposium, ed. E. E. Mamajek, D. R. Soderblom, & R. F. G. Wyse, 345–356
- Basri, G., Walkowicz, L. M., Batalha, N., et al. 2011, *AJ*, 141, 20
- Basri, G., Walkowicz, L. M., Batalha, N., et al. 2010, *ApJ*, 713, L155
- Basri, G., Walkowicz, L. M., & Reiners, A. 2013, *ApJ*, 769, 37
- Basu, S., Grundahl, F., Stello, D., et al. 2011, *ApJ*, 729, L10
- Beck, P. G., Bedding, T. R., Mosser, B., et al. 2011, *Science*, 332, 205
- Beck, P. G., Hambleton, K., Vos, J., et al. 2013, *ArXiv* 1312.4500B
- Beck, P. G., Montalbán, J., Kallinger, T., et al. 2012, *Nature*, 481, 55
- Bedding, T. R., Mosser, B., Huber, D., et al. 2011, *Nature*, 471, 608
- Belkacem, K., Samadi, R., Goupil, M.-J., & Dupret, M.-A. 2008, *A&A*, 478, 163
- Benomar, O., Bedding, T. R., Mosser, B., et al. 2013, *ApJ*, 767, 158
- Benomar, O., Belkacem, K., Bedding, T. R., et al. 2014, *ApJ*, 781, L29
- Borucki, W. J., Koch, D., Basri, G., et al. 2010, *Science*, 327, 977
- Campante, T. L., Chaplin, W. J., Lund, M. N., et al. 2014, *ApJ*, 783, 123
- Campante, T. L., Handberg, R., Mathur, S., et al. 2011, *A&A*, 534, A6
- Ceillier, T., Eggenberger, P., García, R. A., & Mathis, S. 2013, *A&A*, 555, A54
- Chanamé, J. & Ramírez, I. 2012, *ApJ*, 746, 102
- Chaplin, W. J., Basu, S., Huber, D., et al. 2014, *ApJS*, 210, 1
- Chaplin, W. J., Bedding, T. R., Bonanno, A., et al. 2011, *ApJ*, 732, L5
- Chaplin, W. J., Sanchis-Ojeda, R., Campante, T. L., et al. 2013, *ApJ*, 766, 101
- Christensen-Dalsgaard, J. 2008, *Ap&SS*, 316, 13
- Christensen-Dalsgaard, J. 2010, *Astronomische Nachrichten*, 331, 866
- Decressin, T., Mathis, S., Palacios, A., et al. 2009, *A&A*, 495, 271
- Deheuvels, S., Doğan, G., Goupil, M. J., et al. 2014, *ArXiv e-prints*
- Deheuvels, S., García, R. A., Chaplin, W. J., et al. 2012, *ApJ*, 756, 19
- Di Mauro, M. P., Cardini, D., Ventura, R., et al. 2013, in *European Physical Journal Web of Conferences*, Vol. 43, European Physical Journal Web of Conferences, 3012
- do Nascimento, J.-D., da Costa, J. S., & Castro, M. 2012, *A&A*, 548, L1
- Eff-Darwich, A. & Korzennik, S. G. 2013, *Sol. Phys.*, 287, 43
- Eggenberger, P., Meynet, G., Maeder, A., et al. 2010, *A&A*, 519, A116
- Epstein, C. R. & Pinsonneault, M. H. 2014, *ApJ*, 780, 159
- Fröhlich, H.-E., Frasca, A., Catanzaro, G., et al. 2012, *A&A*, 543, A146
- García, R. A., Ceillier, T., Campante, T. L., et al. 2012, in *Astronomical Society of the Pacific Conference Series*, Vol. 462, Progress in Solar/Stellar Physics with Helio- and Asteroseismology, ed. H. Shibahashi, M. Takata, & A. E. Lynas-Gray, 133
- García, R. A., Ceillier, T., Mathur, S., & Salabert, D. 2013a, in *Astronomical Society of the Pacific Conference Series*, Vol. 479, Astronomical Society of the Pacific Conference Series, ed. H. Shibahashi & A. E. Lynas-Gray, 129
- García, R. A., Corbard, T., Chaplin, W. J., et al. 2004, *Sol. Phys.*, 220, 269
- García, R. A., Hekker, S., Stello, D., et al. 2011, *MNRAS*, 414, L6
- García, R. A., Jiménez, A., Mathur, S., et al. 2008a, *Astronomische Nachrichten*, 329, 476
- García, R. A., Mathur, S., Ballot, J., et al. 2008b, *Sol. Phys.*, 251, 119
- García, R. A., Mathur, S., Salabert, D., et al. 2010, *Science*, 329, 1032
- García, R. A., Pérez Hernández, F., Benomar, O., et al. 2014, *A&A*, 563, A84
- García, R. A., Régulo, C., Samadi, R., et al. 2009, *A&A*, 506, 41
- García, R. A., Salabert, D., Mathur, S., et al. 2013b, *Journal of Physics Conference Series*, 440, 012020
- García, R. A., Turck-Chièze, S., Jiménez-Reyes, S. J., et al. 2007, *Science*, 316, 1591
- Gilliland, R. L., Jenkins, J. M., Borucki, W. J., et al. 2010, *ApJ*, 713, L160
- Gizon, L., Ballot, J., Michel, E., et al. 2013, *Proceedings of the National Academy of Science*, 110, 13267
- Goldreich, P. & Keeley, D. A. 1977, *ApJ*, 212, 243
- Goldreich, P., Murray, N., & Kumar, P. 1994, *ApJ*, 424, 466
- Goupil, M. J. 2009, in *Lecture Notes in Physics*, Berlin Springer Verlag, Vol. 765, The Rotation of Sun and Stars, ed. J.-P. Rozelot & C. Neiner, 45–99
- Goupil, M. J., Mosser, B., Marques, J. P., et al. 2013, *A&A*, 549, A75
- Goupillaud, P., Grossmann, A., & Morlet, J. 1984, *Geoeexploration*, 23, 85
- Griffin, R. F. 2007, *The Observatory*, 127, 313
- Haas, M. R., Batalha, N. M., Bryson, S. T., et al. 2010, *ApJ*, 713, L115
- Holdschneider, M., Kronland-Martinet, R., Morlet, J., & Tchamitchian, P. 1989, in *Wavelets*, ed. J. Combes (Springer-Verlag Berlin), 286–297
- Huber, D., Silva Aguirre, V., Matthews, J. M., et al. 2014, *ApJS*, 211, 2
- Jenkins, J. M., Caldwell, D. A., Chandrasekaran, H., et al. 2010, *ApJ*, 713, L120
- Karoff, C., Metcalfe, T. S., Chaplin, W. J., et al. 2013, *MNRAS*, 433, 3227
- Koch, D. G., Borucki, W. J., Basri, G., et al. 2010, *ApJ*, 713, L79
- Lanza, A. F. 2010, in *IAU Symposium*, Vol. 264, IAU Symposium, ed. A. G. Kosovichev, A. H. Andrei, & J.-P. Roelot, 120–129
- Lanza, A. F., Das Chagas, M. L., & De Medeiros, J. R. 2014, *ArXiv* 1402.6691
- Liu, Y., Liang, X. S., & H., W. R. 2007, *Journal of Atmospheric and Oceanic Technology*, 24, 2093
- Mamajek, E. E. & Hillenbrand, L. A. 2008, *ApJ*, 687, 1264
- Marques, J. P., Goupil, M. J., Lebreton, Y., et al. 2013, *A&A*, 549, A74
- Mathis, S. & Zahn, J.-P. 2004, *A&A*, 425, 229
- Mathur, S., Bruntt, H., Catala, C., et al. 2013, *A&A*, 549, A12
- Mathur, S., Eff-Darwich, A., García, R. A., & Turck-Chièze, S. 2008, *A&A*, 484, 517
- Mathur, S., García, R. A., Ballot, J., et al. 2014a, *A&A*, 562, A124
- Mathur, S., García, R. A., Catala, C., et al. 2010a, *A&A*, 518, A53
- Mathur, S., García, R. A., Régulo, C., et al. 2010b, *A&A*, 511, A46
- Mathur, S., Handberg, R., Campante, T. L., et al. 2011, *ApJ*, 733, 95
- Mathur, S., Metcalfe, T. S., Woitaszek, M., et al. 2012, *ApJ*, 749, 152
- Mathur, S., Salabert, D., García, R. A., & Ceillier, T. 2014b, *Journal of Space Weather and Space Climate*, Submitted
- McQuillan, A., Aigrain, S., & Mazeh, T. 2013a, *MNRAS*, 432, 1203
- McQuillan, A., Mazeh, T., & Aigrain, S. 2013b, *ApJ*, 775, L11
- McQuillan, A., Mazeh, T., & Aigrain, S. 2014, *ArXiv* 1402.5694
- Meibom, S., Barnes, S. A., Latham, D. W., et al. 2011a, *ApJ*, 733, L9
- Meibom, S., Mathieu, R. D., & Stassun, K. G. 2009, *ApJ*, 695, 679
- Meibom, S., Mathieu, R. D., Stassun, K. G., Liebesny, P., & Saar, S. H. 2011b, *ApJ*, 733, 115

- Metcalfe, T. S., Chaplin, W. J., Appourchaux, T., et al. 2012, *ApJ*, 748, L10
- Metcalfe, T. S., Creevey, O. L., Dogan, G., et al. 2014, *ArXiv* 1402.3614
- Mosser, B., Barban, C., Montalbán, J., et al. 2011, *A&A*, 532, A86
- Mosser, B., Baudin, F., Lanza, A. F., et al. 2009a, *A&A*, 506, 245
- Mosser, B., Goupil, M. J., Belkacem, K., et al. 2012, *A&A*, 548, A10
- Mosser, B., Michel, E., Appourchaux, T., et al. 2009b, *A&A*, 506, 33
- Nielsen, M. B., Gizon, L., Schunker, H., & Karoff, C. 2013, *A&A*, 557, L10
- Ouazzani, R.-M. & Goupil, M.-J. 2012, *A&A*, 542, A99
- Pace, G. 2013, *A&A*, 551, L8
- Pace, G. & Pasquini, L. 2004, *A&A*, 426, 1021
- Pinsonneault, M. 1997, *ARA&A*, 35, 557
- Pinsonneault, M. 2009, *Nature*, 462, 168
- Pinsonneault, M. H., An, D., Molenda-Żakowicz, J., et al. 2011, *ArXiv* e-prints
- Reese, D. R. 2010, *Astronomische Nachrichten*, 331, 1038
- Reinhold, T. & Reiners, A. 2013, *A&A*, 557, A11
- Reinhold, T., Reiners, A., & Basri, G. 2013, *A&A*, 560, A4
- Skumanich, A. 1972, *ApJ*, 171, 565
- Stello, D., Huber, D., Bedding, T. R., et al. 2013, *ApJ*, 765, L41
- Stello, D., Meibom, S., Gilliland, R. L., et al. 2011, *ApJ*, 739, 13
- Suárez, J. C., Goupil, M. J., Reese, D. R., et al. 2010, *ApJ*, 721, 537
- Thompson, M. J., Christensen-Dalsgaard, J., Miesch, M. S., & Toomre, J. 2003, *ARA&A*, 41, 599
- Thompson, S. E., Christiansen, J. L., Jenkins, J. M., et al. 2013, *Kepler Data Release 21 Notes (KSCI-19061-001)*, *Kepler mission*
- Thygesen, A. O., Bruntt, H., Chaplin, W. J., & Basu, S. 2014, *ArXiv* 1402.3794
- Torrence, C. & Compo, G. P. 1998, *Bulletin of the American Meteorological Society*, 79, 61
- van Saders, J. L. & Pinsonneault, M. H. 2013, *ApJ*, 776, 67
- Zahn, J.-P. 1992, *A&A*, 265, 115

Table 2. Stars for which we can derive a reliable rotation period P_{rot} . KOIs are identified by a \dagger in the KID (*Kepler* IDentification number). The column “Type of detection” explains if P_{rot} has been determined automatically (A) or after a visual check (V). The column “Source of P_{rot} ” gives the set of data – KADACS or PDC – from which the final P_{rot} has been obtained. The * indicates when the KADACS datasets were filtered at 100 days instead of the standard 30 days. This table is available in its entirety in a machine-readable form in the online journal. A portion is shown here for guidance regarding its form and content.

KID	P_{rot} [days]	error P_{rot} [days]	$\langle S_{ph,k=5} \rangle$ [ppm]	error $\langle S_{ph,k=5} \rangle$ [ppm]	Type of detection	source of P_{rot}
1430163	4.16	0.92	223.79	8.18	A	KADACS
1435467	6.68	0.89	208.99	5.81	A	KADACS
2450729	53.00	5.32	164.74	1.78	A	KADACS*
2837475	3.68	0.36	85.68	3.46	A	KADACS
2852862	10.13	0.63	123.90	3.33	A	KADACS
2865774	6.22	0.56	141.49	5.49	V	PDC
2998253	6.79	0.53	180.04	5.90	A	KADACS
3112152	15.48	1.19	180.25	4.11	V	KADACS
3123191	20.33	1.38	332.06	5.29	A	KADACS
3223000	4.85	0.39	1096.52	34.88	A	KADACS
3236382	3.66	0.42	99.56	4.40	V	PDC
3241581	26.26	2.01	177.18	2.65	V	KADACS
3344897	5.66	0.94	268.28	8.52	A	KADACS
3424541	3.46	0.33	322.94	12.57	A	KADACS
3430893	8.29	0.69	123.11	3.65	A	KADACS
3632418 \dagger	12.89	1.38	133.50	2.71	A	KADACS
3633847	10.96	1.03	122.10	3.01	A	KADACS
3633889	4.23	0.30	52.90	2.71	A	KADACS
3642422	48.73	8.19	259.91	2.92	V	PDC
3643774	14.40	1.56	223.65	4.36	A	KADACS
3656476	31.67	3.53	80.90	1.48	A	KADACS
3657002	16.02	1.54	201.59	4.00	A	KADACS
3661135	28.39	4.83	174.53	3.10	A	KADACS
3733735	2.56	0.19	251.21	11.65	A	KADACS
...						

Table 3. Table of the multiple stars in our sample. Columns are the same as in Table 2 except for the column “Type” in which the type of multiple star is given (EB: eclipsing binary, SB2: double-lined spectroscopic binary, Mult: multiple in SIMBAD database, Seis/Pol: seismic binary or pollution by a nearby red giant) and the column “Reference” which explains from which paper or website this classification comes from. Stars for which no rotation period was derived have $P_{\text{rot}} = \langle S_{ph,k=5} \rangle = -1$. The star which KID shows a \dagger is a KOI.

KID	P_{rot} [days]	error P_{rot} [days]	$\langle S_{ph,k=5} \rangle$ [ppm]	error $\langle S_{ph,k=5} \rangle$ [ppm]	Type	Reference
2010607	17.60	3.89	264.73	5.06	EB	Kirk et al. 2013, in prep.
3427720	13.94	2.15	106.72	2.27	Mult.	SIMBAD
4586099	10.76	1.94	137.62	3.25	Mult.	SIMBAD
5021689	-1.00	0.00	-1.00	0.00	Mult.	SIMBAD
7510397	-1.00	0.00	-1.00	0.00	Mult.	SIMBAD
7938112	0.84	0.07	214.08	19.03	Seis/Pol	This study
8360349	-1.00	0.00	-1.00	0.00	Mult.	SIMBAD
8379927	16.99	1.35	1340.50	23.44	SB2	Griffin 2007
9025370	13.31	1.30	171.69	3.63	SB2	Thygesen et al. 2014
9139151	10.96	2.22	187.29	4.22	Mult.	SIMBAD
9139163	6.10	0.47	71.23	2.32	Mult.	SIMBAD
9693187	-1.00	0.00	-1.00	0.00	SB2	Thygesen et al. 2014
9908400	17.12	1.26	530.12	10.29	Mult.	SIMBAD
10124866	17.59	2.27	248.23	4.38	Mult.	SIMBAD
11453915 \dagger	23.85	1.55	75.45	1.38	EB	Kirk et al. 2013, in prep.

Table 4. Table of the stars for which we see no sign of rotation in the lightcurve. The star which KID shows a \dagger is a KOI.

KID
4915148
4918355
5603483
5629080
8179973 \dagger
8547279